THE JOURNAL OF PHYSICAL CHEMISTRY B

Article

pubs.acs.org/JPCB

Interfacial Growth of Controllable Morphology of Silver Patterns on Plastic Substrates

Guanghui Cui,[†] Shengli Qi,[†] Xiaodong Wang,[†] Guofeng Tian,[†] Guang Sun,[†] Wei Liu,[†] Xiaona Yan,[†] Dezhen Wu,[†] Zhanpeng Wu,*[,†] and Li Zhang*[,‡]

[†]Key Laboratory of Carbon Fiber and Functional Polymers, Ministry of Education, Beijing University of Chemical Technology, Beijing 100029, P. R. China

[‡]CAS Key Laboratory of Colloid, Interface and Chemical Thermodynamics, Institute of Chemistry, Chinese Academy of Sciences, Beijing, 100190, P. R. China

Supporting Information

ABSTRACT: Controllable growth of newly born silver nanoparticles to fractal, cauliflower-like, microscale disks and continuous silver layers with high conductivity and reflectivity on plastic substrates has been developed via solid−liquid interfacial reduction and growing of ion-doped polymeric films. Such approaches involve polyimide (PI) films as substrates, its corresponding silver-ion-doped precursors as solid oxidants, and facile immersion of ion-doped polymeric films in aqueous reducing solution. The solution reducing process belongs to liquid−solid interfacial reduction processes, during which silver ions doped in polymeric matrix transformed to newly born silver nanoparticles which further aggregated and migrated along the liquid−solid interface to form dendrite, cauliflower-like and lamella disk-like architecture and/or severely compact continuous silver nanolayers with highly reflective and conductive properties. Time-dependent morphology evolutions of silver particles were traced by scanning electron microscopy (SEM), atomic force microscopy (AFM), and transmission electron microscopy (TEM). This strategy can also extend to synthesis of many other metals on polymeric films while maintaining outstanding metal−polymer adhesion based on incorporation of various metal ions, and may offer an opportunity to fabricate large scale, high-output, cost-effective processes for metal patterns on flexible polymeric substrates.

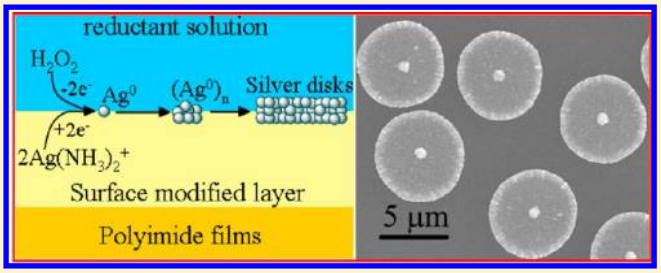

1. INTRODUCTION

The fabrication of metal crystals on plastic films has attracted considerable attention owing to its property combination effects because plastic substrates possess many attractive properties including flexibility, lightweight, shock resistance, and softness.[1,2] Among the variety of polymeric substrates, polyimide (PI) is a promising candidate because of its attractive properties including excellent high thermal stability, dielectric constant, and good resistance to organic solvents.[3−7] Because of the high electrical conductivity and excellent reflectivity of silver metal, it is of considerable interest in modern science and technology for applications as diverse as plasmonics,[8] photics and photonics,[9] sensors,[10] catalysis,[11] reflector and antibacterial.[12]

During past decades, much interest and efforts have been focused on shape- and size-controlled synthesis of silver nanocrystals on polymeric surface in order to adjust the functional properties of the composite films. However, it still remains a great challenge of control of orders of silver microstructures while maintain good adhesion properties between silver and PI interfaces. Conventional approaches for metallization on the polyimide surfaces, such as physical vapor deposition (PVD) and chemical vapor deposition (CVD), can fabricate the films with controllable microstructure of silver crystals. A major drawback of these methods is the poor adhesion of silver layers on the underlying polymer substrate.[13] To enhance the adhesion property, the self-metallization technique has been proposed and developed by Southward,[14] Taylor,[15] Warner,[16] Matsuda,[17] Sawada,[18] et al. This method refers to developing a metallized film from a single homogeneous solution that contains both an organometallic silver complex and a polyimide precursor, poly(amic acid) (PAA). Thermal treatment of the casted film converts the precursor into the final polyimide form with concomitant silver reduction yielding silvered polyimide film. However, the most used silver(I) precursors are expensive fluorine containing silver(I) precursors, such as hexafluoroacetylacetonato silver(I) and trifluoroacetylacetonato silver(I), which would inevitably increase the cost of the final products.

Recently, our group developed a direct ion-exchange self-metallization process using facile and modest cost of silver salts, such as silver nitrate, as the silver precursor and synthetic poly(amic acid) (PAA) as the polyimide precursor which owe ion-exchangeable sites. Silver ions are doped into the PAA

Received: May 24, 2012
Revised: August 21, 2012
Published: September 27, 2012

matrix via ion exchanging of damp-dry PAA films in aqueous silver nitrate solutions, and heat treatment of the silver-doped precursor films leads to cyclization of PAA to PI, and simultaneous reduction of silver ions, forming continuous silver layers on polyimide films with reflective and conductive properties.[20−22] However, the morphology of the silver layer is very difficult to control due to the thermal curing processes which cause drastic aggregation of newly born silver nanoparticles to island growth. What is worse, the thermal treatment causes a severely burnt out effect of final films because newly formed silver nanoparticles via thermal treatment possess strongly catalyze a decomposition effect and the spontaneous aggregation of silver nanoparticles released vast heat which further enhances decompostion of its surrounding PI substrates.[23]

In fact, the surface of commercial PI films can change into the ion exchangeable precursors via base hydrolysis reaction because the ion-doped precursors have triggered the development of a new concept in metallization of polymer substrates. A variety of techniques have been developed by several groups, on the basis of thermal treatment,[19−23] photoinduced chemistry,[24−26] and chemical reduction[27−30] for metallization of polyimides. However, there are several drawbacks that need to be overcome. For instance, the pyrolysis phenomena of the silvered polyimide films have been found via the thermal treating process. More recently, we have developed a low-temperature processable technique to fabricate PI/Ag films with reflective and conductive properties via immersing silver ion doped films into the alkali glucose solution for the reduction reaction.[29] However, the mechanism of diffusion and aggregation of silver and/or silver ions at interfaces has not yet been revealed.

Herein, as a continuation to the metallization of the polyimide surfaces described in our previous paper, the present work mainly reports on how to precisely control and to understand the reducing reaction process of silver ions and aggregation of silver nanoparticles at liquid−solid interfaces at room temperature. The procedure is outlined in Scheme 1. Ion-exchangeable sites, poly(amic acid) layer, were obtained via immersion of commercial PI films in aqueous KOH solution to conduct hydrolysis reaction, and ion exchange process in aqueous $[Ag(NH_3)_2]OH$ solution. Subsequently, the films were immersed into the various reducing agent aqueous solutions during which double diffusion and reduction processes might occur between the interfaces of silver ions and/or newly born silver crystals in doped polymeric films and the aqueous reducing surroundings. In order to clearly investigate the growing process of newly born silver nanoparticles at the solid−liquid interfaces, hydrogen peroxide, hydroquinone, and hydrazine solutions which have relatively weak reducing power were chosen as reducing agents, along with their corresponding comparing reductants such as copper sheets and particles. We believe that aggregation effects of newly born silver nanoparticles can be traced via SEM and AFM measurement. We demonstrate in this study how it is possible to explain that newly born silver nanoparticles merge into fractal, cauliflower-like, microscale disks and continuous silver layers with high conductivity and reflectivity on plastic substrates while maintaining unique silver-polymer adhesive property. This fabrication method is expected to extend to the large scale roll-to-roll fabrication technique, and the resulting ideal micro/nanostructure with functionalized metallized surfaces could provide a potential platform for microelectronic devices, optical switches, and flexible mirrors.

Scheme 1. Ideal Illustrative Procedures for Controllable Interfacial Growth Silver Microdisks and Nanolayer on Polyimide Surface in Aqueous Solutions at Room Temperature

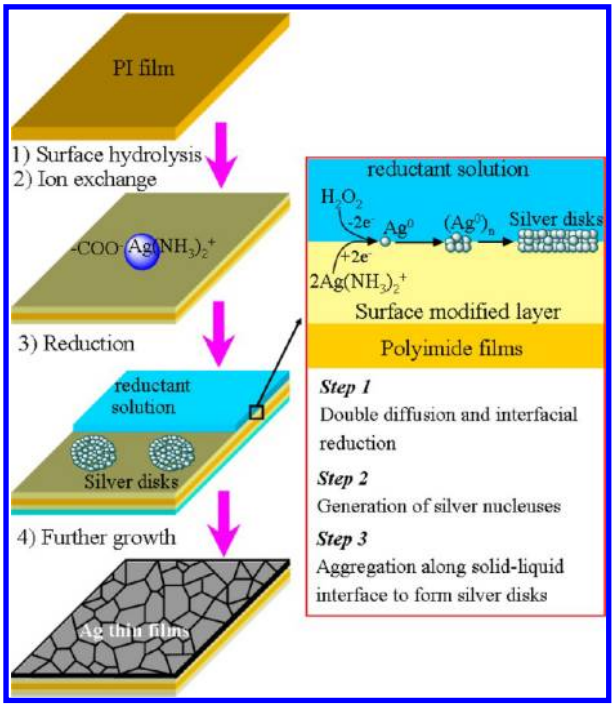

2. EXPERIMENTAL SECTION

2.1. Materials. Commercial pyromellitic dianhydride oxidianiline (PMDA-ODA) polyimide films with a thickness of 75 μm were obtained from Shanghai QianFeng Insulating Material Plant (P.R. China). The surface of the film was rinsed by ultrasonic cleaning for 5 min in deionized water and dried in an ambient environment prior to use. Hydrogen peroxide (H_2O_2), hydroquinone, hydrazine, aqueous ammonia, KOH, and $AgNO_3$ were purchased from Beijing Chemical Company and used as received (analytically pure).

2.2. Growth of Silver Microdisks to Continuous Silver Nanolayers on PI Films. The whole process mainly involved three steps: abluent bare polyimide films were first immersed into 3 M aqueous KOH solution for several minutes and then rinsed carefully with deionized water. KOH-treatment of the pristine polyimide can induce imide rings cleaved to form potassium salts of carboxylic acid and amide bonds. Then, the surface-modified polyimide films were inserted into aqueous $[Ag(NH_3)_2]OH$ solution for several minutes to perform cation-exchange reaction, and then washed again with a copious amount of deionized water. In this step, silver ions replaced the potassium ions and were incorporated into the modified layer of polyimide film. Finally, the silver-ion-doped polyimide films were immersed into various reductant solutions such as hydrogen peroxide, hydroquinone, and hydrazine hydrate solutions for certain seconds to reduce the silver ammonia complex ions to silver nanoparticles and aggregate to disk-like morphology. The schematic illustration was presented in Scheme 1.

dx.doi.org/10.1021/jp305060u | J. Phys. Chem. B 2012, 116, 12349−12356

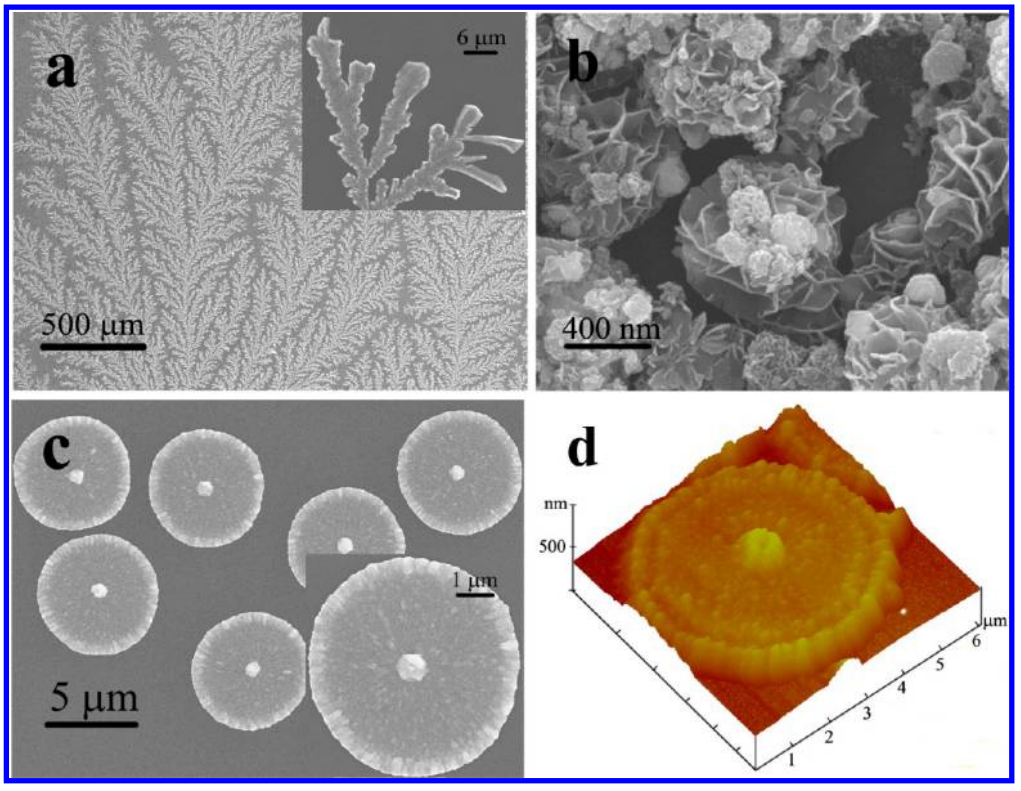

Figure 1. SEM images of the samples with various morphologies: (a) fractal patterns, (b) cauliflower-like structures, and (c) microdisks structures. (d) was the 3D AFM image corresponding to a single microdisk in (c). The samples were obtained by etching in 3 M KOH solution for 3 h, ion-exchange in 0.1 M $[Ag(NH_3)_2]OH$ solution for 10 min, and final reduction in various conditions: (a) using copper sheets in deionized water as reductant, (b) using copper microspheres in deionized water as reductant, and (c) using 0.23 mmol/L H_2O_2 solution for about 3 s. The insets are the close view of the treetop and a single Ag microdisk with higher magnifications.

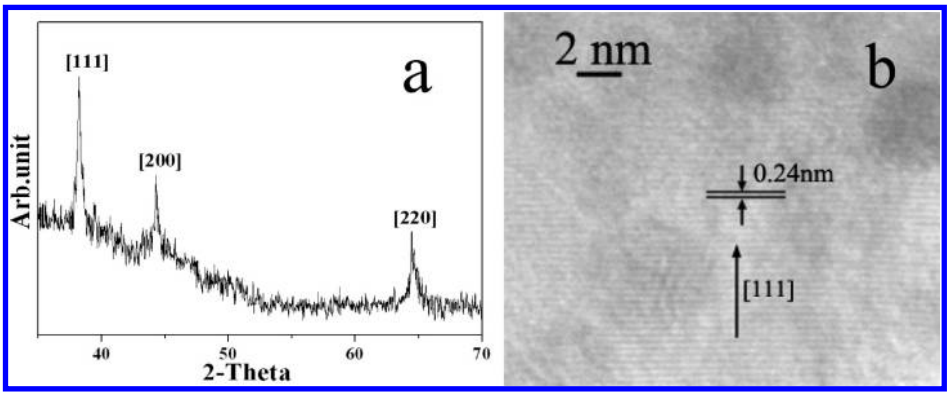

Figure 2. A typical XRD pattern (a) and HRTEM image (b) of the Ag microdisks. The sample was obtained by etching in 3 M KOH solution for 3 h, ion-exchange in 0.1 M $[Ag(NH_3)_2]OH$ solution for 10 min, and final reduction in 0.23 mmol/L H_2O_2 solution for about 3 s.

2.3. Growth of Silver Dendrites and Cauliflower-Like Structures. The process to grow silver dendrites and cauliflower-like structures was similar to that of growth of silver microdisks and/or reflective mirrors on polyimide films except for the final reducing process. In the final step, copper sheets and particles in deionized water were used as solid reductants for several hours to weeks in a dark environment.

2.4. Characteriation. X-ray diffraction (XRD) was performed on an X-ray diffractometer (D/Max2500 VB2+/PC, Rigaku, Japan). The X-ray beam was generated by a Kα target, and the diffractograms were recorded in the 5−90° region. The morphology was observed by scanning electron microscopy (SEM, Hitachi S4800) and atomic force microscopy (AFM, Digital Instruments Inc. of Santa Barbara, CA). AFM images were collected using a Nanoscope IIIa in tapping mode in air with a scanning rate of 0.9 Hz. All SEM and AFM images were collected on the upside of films. Transmission electron microscopy (TEM) was performed on an H-800 type Hitachi instrument at an operating voltage of 200 kV. The samples were prepared by adhering the film on a polyvinyl chloride board followed by cutting it perpendicular to the film surface using an ultramicrotome. These thin sections floating on a water bath were mounted onto the carbon-coated TEM copper grids for analysis. The HRTEM images were obtained using the JEOL JEM-3010 with an acceleration voltage of 200 kV. A SDY-4 four-point probe instrument (Guangzhou, China) was employed to measure the electrical resistivity of two surfaces of the silvered PI films. Reflectivity spectra (relative to

dx.doi.org/10.1021/jp305060u | J. Phys. Chem. B 2012, 116, 12349−12356

a $BaSO_4$ mirror set at 100% reflectivity) were scanned on a Shimazu 2501 PC UV/vis spectrophotometer in the 200−800 nm wavelength range. The values at 531 nm were chosen to represent the films' reflectance in the visible region. The optical photos of films were taken by Fujifilm S8000.

3. RESULTS AND DISCUSSION

3.1. Effects of Reduction Conditions on Silver Morphology. The main reaction in preparation of various silver morphologies through the solid−liquid interfacial process involved the reduction of silver ions at the interfaces of ion-doped polymeric surface and reducing agents containing solutions at room temperatures, as shown in the right part of Scheme 1. During the initial stage of the reduction process, after the ion-doped films were dipped into aqueous reduction solution, silver ions were reduced into neutral atoms that then aggregate and evolve into nanoscale and/or mesascale crystals on polyimide films. Morphologies of silver superstructures, such as microdisks, fractal, cauliflower-like, were controllable depending on reductants and reducing surroundings. As shown in Figure 1a, a dendritic structure morphology formed when solid reductants such as copper or ion sheets were put into aqueous solution. Or, alternatively, when copper or ion sheets were replaced by their corresponding solid microspheres, a "flower-like" pattern would form instead of a corresponding dendritic silver pattern, as shown in Figure 1b. We suggest that newly born silver nanoparticles are likely to aggregate in a diffusion-controlled manner, and accordingly, dendritic growth may occur if the silver nanoparticles are allowed to diffuse by Brownian motion.[31] The diffusion-controlled process would happen if the formation rate of newly born silver nanoparticles decreased, which can be controlled by controlling over the releasing rate of reducing electrons. The silver crystals with disk-like shape were evolved only if soluble reductants were utilized to conduct the liquid−solid interfacial reaction. When the ion-doped films were dipped into aqueous reduction solutions, such as hydrogen peroxide, hydroquinone, and hydrazine hydrate solutions for several seconds, silver ions reduced rapidly to form silver nanoparticles and these silver nanoparticles can serve as seeds and nuclei during next reduction and growing processes. Herein, aqueous H_2O_2 solution was selected as the reducant for its relatively weaker reducing power in comparison with other reductants such as glucose,[29] DMAB,[30] hydrazine hydrate, and hydroquinone (Figures S1 and S2, Supporting Information). Then, we can slow down effects of combination and aggregation of newly born silvers, making it possible to observe the evolution processes of silver microdisks by SEM and AFM, which was indispensable to give a possible mechanism of forming continuous silver layers on polymeric substrates. We will discuss the evolution of silver microdisks at the interfaces of the solid (the ion-doped films) and solution phases in more detail below.

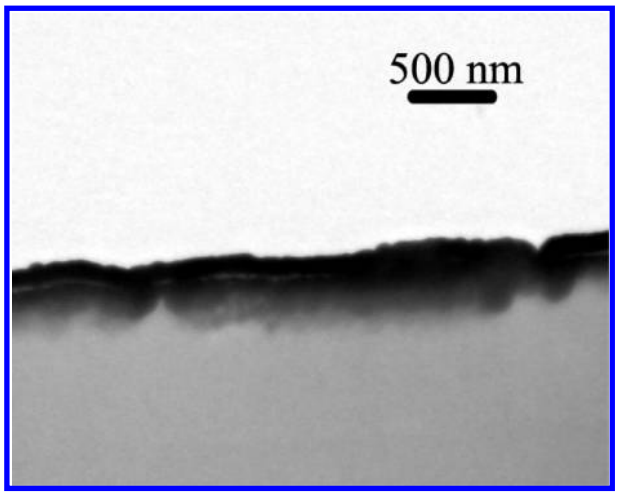

Figure 3. TEM images of the silvered films which is the same sample as that in Figure 2.

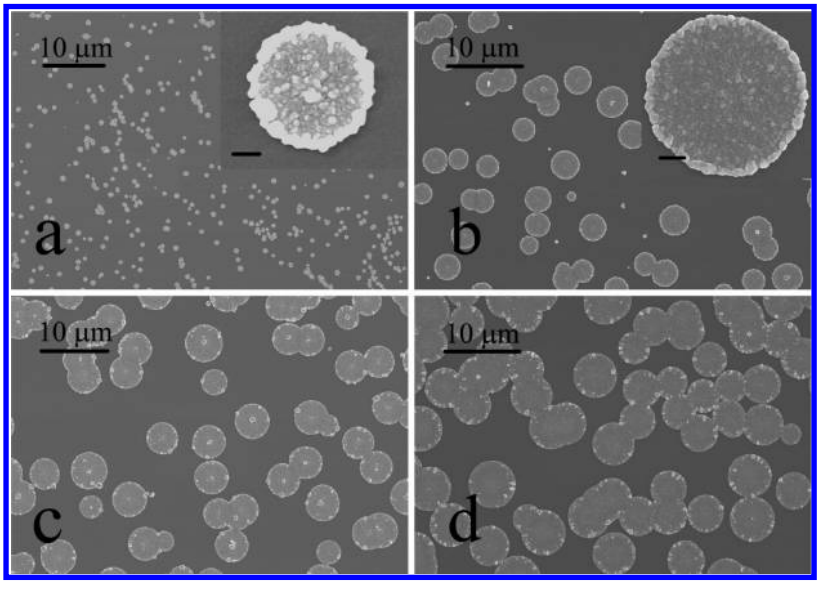

Figure 4. SEM images: the samples were obtained by etching in 3 M KOH solution for 3 h, ion-exchange in 0.1 M $[Ag(NH_3)_2]OH$ solution for 10 min, and final reduction at ~0 °C in 0.016 mmol/L H_2O_2 solution for about (a) 1 s, (b) 5 s, (c) 10 s, and (d) 20 s. The inset is the close view of Ag microdisks with higher magnifications. The scale bar in the inset corresponds to 600 nm. The corresponding diameter distributions were shown in Figure S3 (Supporting Information).

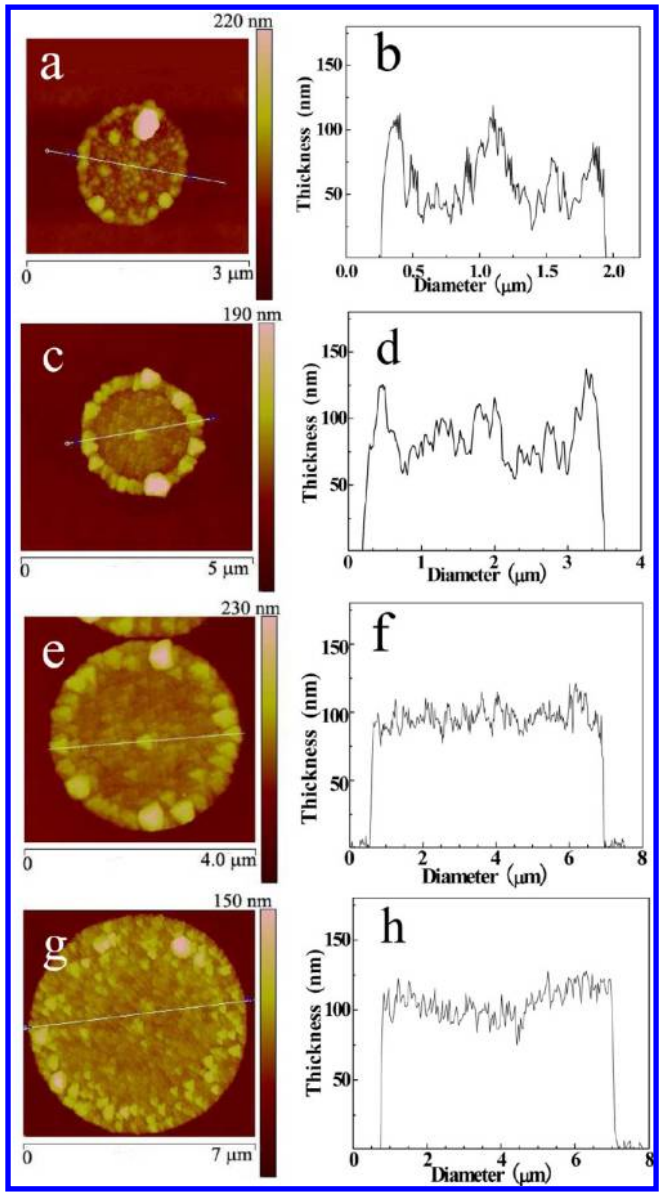

Figure 5. 2D AFM images: the samples were obtained by hydrolyzation in 3 M KOH solution for 3 h, ion-exchange in 0.1 M $[Ag(NH_3)_2]OH$ solution for 10 min, and final reduction at ~0 °C in 0.016 mmol/L H_2O_2 solution for about (a) 1 s, (c) 5 s, (e) 10 s, and (g) 20 s. (b), (d), (f), and (h) are the height profiles along the corresponding lines responding to (a), (c), (e), and (g), respectively.

Figure 1c and 1d shows SEM and AFM images of typical silver microdisks on polymer substrate for the sample immersing in 3 M KOH solution for 3 h, ion-exchange in 0.1 M $[Ag(NH_3)_2]OH$ solution for 10 min, and final reduction in 0.23 mmol/L H_2O_2 solution for about 3 s. As shown in Figure 1c, one can clearly observe that the silver architecture is uniform in shape: well-rounded disk shapes with a larger silver particle in the center of a circle. A close view of one single microdisk reveals that it consists of numerous aggregated nanoparticles and has a nanoroughened surface. The AFM 3D image in Figure 1d shows that the microdisks were assembled from smaller silver nanoparticles, which is consistent with the result of magnified SEM images. The average diameter (D) and thickness (t) of the microdisks have been estimated as 5 μm and 100 nm, respectively, corresponding to an approximate aspect ratio of D/t = 50, which is much larger than that reported elsewhere,[32−34] indicating the lamella structures of the resultant silver microdisks.

3.2. Formation of Silver Microdisks. The initial reduction process results in the concentration gradient of silver ions in the direction perpendicular to the film's surface. On one hand, silver ions doped in the modified layers would diffuse outward toward interfaces because of their concentration gradient, suggesting a well-defined controlled release process and continuous supplement of silver ions for the next reduction and growth process. On the other hand, the liquid reductant molecules may also diffuse into the modified layers. Ostwald ripening theory suggests that the newly born silver atoms or nanoparticles are unstable because of their high surface free energy. They would spontaneously aggregate and deposit to each other around one nucleus. However, aggregation behaviors of the silver nanoparticles can only migrate along the liquid−solid interface which acts as the two-dimensional restrictive cues,[35] and form round and lamella architectures with large aspect ratio, which has the smallest surface free energy on a two-dimensional plane. Figure 2 shows the crystalline nature of the silver microdisks which was examined by XRD and HRTEM analysis. As shown in Figure 1a, all the diffraction peaks observed can be assigned to the {111}, {200}, and {220} diffraction peaks of the face-centered cubic (fcc) structure of metallic Ag, respectively. The measured lattice spacing of 0.24 nm from the HRTEM in Figure 1b matches Ag {111}, which is in agreement with the XRD result.

Figure 3 shows the cross-sectional TEM image of the same sample in Figure 2. We can observe that the silver layer with a thickness of approximate 300 nm was formed on the surface of a polymeric substrate and the gap in the silver layers indicated

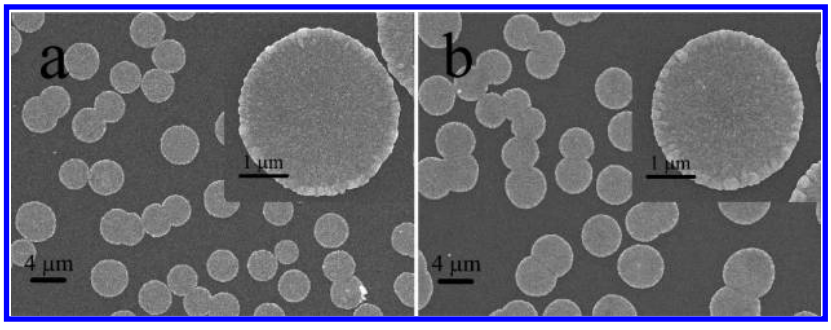

Figure 6. SEM images: the samples were obtained by etching in 3 M KOH solution for 0.5 h, ion-exchange in 0.1 M $[Ag(NH_3)_2]OH$ solution for 10 min, and final reduction in 0.016 mmol/L H_2O_2 solution for about (a) 5 s and (b) 180 s, at about 20 °C. The insets are the close view of Ag microdisks with higher magnification.

dx.doi.org/10.1021/jp305060u | J. Phys. Chem. B 2012, 116, 12349−12356

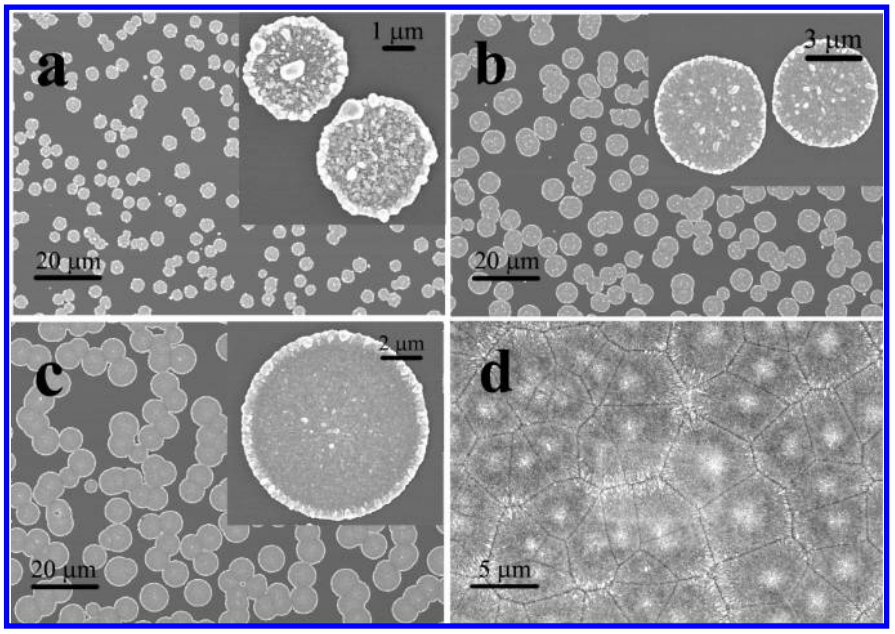

Figure 7. SEM images: the samples were obtained by etching in 3 M KOH solution for 3 h, ion-exchange in 0.1 M $[Ag(NH_3)_2]OH$ solution for 10 min, and final reduction in 0.16 mmol/L H_2O_2 solution for about (a) 1 s, (b) 3 s, (c) 5 s, and (d) 20 s, at about 0 °C. The insets are the close view of Ag microdisks with higher magnification.

Table 1. Conductivity and Reflectivity Dates of the Samples with Various Reduction Conditions

	reducing conditions in H_2O_2 solution at different temperatures					
	0.016 mmol/L at 0 °C		0.16 mmol/L at 0 °C		0.16 mmol/L at 20 ° C	
reduction time (s)	surface resistivity (Ω/sq)	reflectivity (%)	surface resistivity (Ω/sq)	reflectivity (%)	surface resistivity (Ω/sq)	reflectivity (%)
1	NC[a]		NC	14.5	PC	19.1
3	NC		PC	37.2	307	49.7
5	NC		390	48.2	38	56.7
7	NC		421	52.2	11	72.2
10	NC		190	61.5	0.1	99.0
15	NC		27	76.3	0.2	95.1
20	PC[b]	39.5	0.3	98.5	0.5	97.4
30	PC	42.3	0.2	98.1	0.5	96.2
60	PC	38.7	0.5	96.6	0.7	94.9

[a]NC = not conductive. [b]PC = partially conductive.

the aggregation defects of silver nanoparticles. These results suggest the formation of a different morphology of silver mesoscale and/or macroscale transformation process is that the aggregates are not single crystals but energy-minimized architectures of a great number of nanoparticles. This is in contrast to thermal methods for uncontrolled particle sizes on polyimide films, in which silver nanoparticles typically lead to aggregation with island-growth-like rough morphology on surfaces of the films, and aggregation of silver nanoparticles would release a lot of heat which would result in degradation of polyimide through carbonization (pyrolysis) of the matrix at high temperatures.[23,36]

3.3. Effect of Reduction Time on the Growth of Silver Microdisks. The time-dependent morphology of such Ag microdisks was traced by SEM and AFM measurements, which were shown in Figures 4 and 5. The samples were prepared by reducing in 0.016 mmol/L H_2O_2 solution for different times. In all cases, it was clear that epitaxial growth of silver microdisks on the polymeric substrates generated similar disk-like morphologies with continuously increasing diameters and thicknesses. Specifically, after reduction for about 1 s in H_2O_2 solution, no obvious difference in appearance of the silver-doped films could be observed by our naked eyes. However, SEM images showed that a great number of silver microdisks with diameters ranging from 500 nm to 2.1 μm have grown on the surface, which can be clearly confirmed in the inset of Figure 4a and Figure S3 (Supporting Information). Both the corresponding 2D AFM image and height profiles in Figure 5a and 5b confirm that the surface of the newly formed silver microdisks was quite rough, which could be possibly attributed to the aggregation of numerous silver nanoparticles. We presume that the nanoparticle in the center of a silver microdisk (the elemental component of which is shown in Figure S4, Supporting Information) probably acted as the nucleus during the initial aggregation growth of silver nanoparticles. Prolonging the reducing reaction time to 5 s enabled the newly born silver nanoparticles to aggregate, which led to the similar outline of those silver microdisks but with an apparent increase in the diameters ranging from ca. 2 to 4 μm. Further reduction to about 20 s led to the further growth of silver microdisks of diameters ranging from ca. 4 to 7 μm and some neighbor silver microdisks grew to bond together with

dx.doi.org/10.1021/jp305060u | J. Phys. Chem. B 2012, 116, 12349−12356

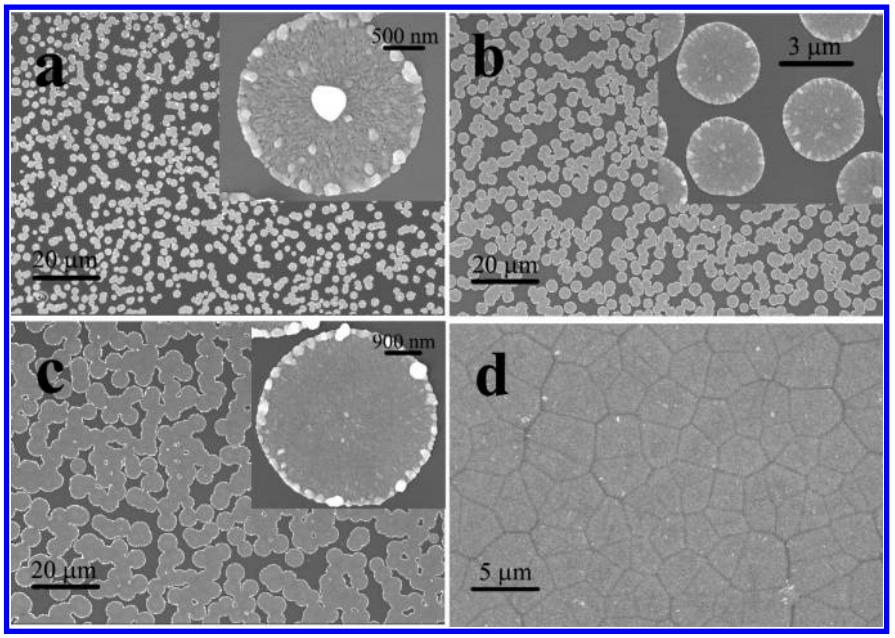

Figure 8. SEM images: the samples were obtained by etching in 3 M KOH solution for 3 h, ion-exchange in 0.1 M $[Ag(NH_3)_2]OH$ solution for 10 min, and final reduction in 0.16 mmol/L H_2O_2 solution for about (a) 1 s, (b) 3 s, (c) 5 s, and (d) 10 s, at about 20 °C. The insets are the close view of Ag microdisks with higher magnification.

each other. The surface silvered films became partly conductive because the close knit silver microdisks formed an electrically conductive path. The corresponding AFM image in Figure 5g shows that the surface of the silver microdisk became smoother than that with short reducing time, indicating that the silver microdisks tend to merge more ordered structures.

3.4. Effect of Silver Loadings on the Growth of Silver Microdisks. Our previous research showed that the silver ions loading content in the modified layer linearly depends on the initial KOH treatment time.[29] The silver loadings play an important role in determining the time-dependent morphology evolutions. When the initial KOH treatment was 0.5 h and reduced for 5 s in the 0.016 mmol/L H_2O_2 solution, as shown in Figure 6a, well-defined silver microdisks with an average diameter of about 4.5 μm could be formed on the film surface and only a few neighbor silver microdisks grew bonding together. When the reducing reaction time was prolonged to 180 s, the number of and morphologies of the silver microdisks remained unchanged, which suggested that silver loadings in the modified layers was not enough for the microdisks to grow bigger even with long reduction time; thus, we can control the number and the size of the silver microdisks on the film surface by controlling the initial hydrolyzation time.

3.5. Effects of Reduction Conditions on Properties of the Surface Silvered Films. The growth processes of silver microdisks can also be controlled by changing the concentrations and temperatures of the H_2O_2 solution. Figure 7 shows the SEM images of the samples which were obtained by hydrolyzation in 3 M KOH solution for 3 h, ion-exchange in 0.1 M $[Ag(NH_3)_2]OH$ solution for 10 min, and final reduction in 0.16 mmol/L H_2O_2 solution for about (a) 1 s, (b) 3 s, (c) 5 s, and (d) 20 s, at about 0 °C. Although similar disk-like morphologies with increasing diameters have been observed in a concentrated H_2O_2 solution, high concentrations of reductant solution can accelerate the growth process of silver nanoparticles remarkably, compared with the silver microdisks that reduced in 0.016 mmol/L H_2O_2 solution. For the film reduced in 0.16 mmol/L H_2O_2 solution for about 1 s, as shown in Figure 7a, no conductivity of the films could be detected and its reflectivity was very low, ~14.5%, as shown in Table 1, because these silver microdisks were isolated from each other and no continuous silver layers were formed on the surface of films. Prolonging the reducing reaction time to 3 s, the average diameters ascended to about 6 μm. The films became partly conductive and the reflectivity could reach about 37.2%. When the reducing reaction time was 5 s, the silver microdisks grew larger and some neighbor disks became bonded together. The conductivity and reflectivity of the films meliorated moderately with a surface resistivity of ~390 Ω/sq and reflectivity of 48.2%. Interestingly, as the reducing reaction time increased to 20 s, the close knit silver microdisks grew further to form a mirror-like continuous silver layer with high reflectivity and conductivity, as shown in Figure 7d. The films presented with silver metallic luster (Figure S5, Supporting Information). Both conductivity and reflectivity of the films meliorated remarkably. The surface reflectivity could be detected up to ca. 98.5%, and the surface resistivity could be as low as ca. 0.2 Ω/sq, which was similar to conductivity and reflectivity of pure silver mirrors. The flexible plastic substrate with reflective and conductive layers has great interest for application in the fields of microelectronic and aerospace industry. Figure 8 shows the SEM images of the samples which were reduced at high temperature, ~20 °C. Comparing to that in Figure 7, it is obviously that higher reduction temperature can accelerate the reduction and growth speed of silver nanoparticles. Specifically, it took 20 s to form continuous silver nanolayers on the surfaces of substrate film at 0 °C, while it was only 10 s at 20 °C. SEM shows that the silver layers present distinctly ideal "bubbles" like compacted structure. Such kinds of materials with most effective subdivision of three-dimensional structures were calculated by many researchers including the great physicist Lord Kelvin. Self-assembly structure mediated by van der Waals forces and hydrophobic interactions led primarily to close-packed structures such as ideal structure and unique

dx.doi.org/10.1021/jp305060u | J. Phys. Chem. B 2012, 116, 12349−12356

performances can be achieved when the assembly process was confined to a liquid−solid interface which can help control the placement of nanoscopic, mesoscopic, and macroscopic building blocks.[37,38] In nature, we can also see many of these phenomena such as the assembly of red blood cells, water bubbles, and honeycombs.

CONCLUSIONS

Well-defined fractal, cauliflower-like, microscale disks and continuous silver layers with high conductivity and reflectivity could be fabricated on the surface of polyimide films via a novel interfacial growth technique at room temperature, which involved the double diffusion of silver ions in the modified layer, and reduction reactions at the interfaces between solid substrate and reductant molecules. The sizes and morphologies of silver microdisks could be controlled by the silver loadings and reduction conditions, such as time, concentration, and temperature. Silver microdisks would evolve into ideal compacted silver patterns on polymeric films depending on enough silver ion loadings in films and appropriate reduction conditions. The continuous and smooth silver layers present excellent surface resistivity (0.2 Ω/sq) and high reflectivity (99%). In addition, because of the convenience of the procedure and the ready availability of the chemicals used in this work, this route is expected to be applicable to a variety of growth of noble metal, metal oxide, and sulfide crystals on polymeric substrates by tuning species of metal ions and appropriate countra-ions, which may offer a new electroless process for the microfabrication of flexible functional composite films.

ASSOCIATED CONTENT

Supporting Information

Supporting figures of the samples reduced by hydrazine hydrate and hydroquinone solutions, the diameter distributions corresponding to Figure 4, EDS analyses, and digital photographs of bare PI film and the surface-silvered PI film. This material is available free of charge via the Internet at http://pubs.acs.org.

AUTHOR INFORMATION

Corresponding Author

*E-mail: wuzp@mail.buct.edu.cn (Z.W.); zhangli@iccas.ac.cn (L.Z.).

Notes

The authors declare no competing financial interest.

ACKNOWLEDGMENTS

This research was financially supported by the National Natural Science Foundation of China (NSFC, Project 50973006) and the Program for Changjiang Scholars and Innovative Research Team in University (PCSIRT, IRT0706).

REFERENCES

(1) McAlpine, M. C.; Ahmad, H.; Wang, D. J.; Heath, R. *Nat. Mater.* **2007**, *6*, 379−284.
(2) Homan, K. A.; Chen, J. A.; Schiano, M.; Willets, K. A. *Adv. Funct. Mater.* **2011**, *21*, 1536−1540.
(3) French, B. L.; Davis, L. M.; Munzinger, E. S.; Christy, P. C.; Thompson, D. W.; Southward, R. E. *Chem. Mater.* **2005**, *17*, 2091−2100.
(4) Akamatsu, K.; Ikeda, S.; Nawafune, H.; Yanagimoto, H. *J. Am. Chem. Soc.* **2004**, *126*, 10822−10823.
(5) Thompson, D. S.; Davis, L. M.; Thompson, D. W.; Southward, R. E. *ACS Appl. Mater. Interfaces* **2009**, *1*, 1457−1466.
(6) Qi, S.; Wu, Z.; Wu, D.; Jin, R. *J. Phys. Chem. B* **2008**, *112*, 5575−5584.
(7) Dow, W. P.; Liao, G. L.; Huang, S. E.; Chen, S. W. *J. Mater. Chem.* **2010**, *20*, 3600−3609.
(8) Tao, A.; Sinsermsuksakul, P.; Yang, P. *Nat. Nanotechnol.* **2007**, *2*, 435−440.
(9) Stamplecoskie, K. G.; Scaiano, J. C. *J. Am. Chem. Soc.* **2010**, *132*, 1825−1827.
(10) Trefry, J. C.; Monahan, J. L.; Weaver, K. M.; Arnold, Z. S.; Wooley, D. P.; Pavel, I. E. *J. Am. Chem. Soc.* **2010**, *132*, 10970−10972.
(11) Lei, Y.; Mehmood, F.; Lee, S.; Greeley, J.; Lee, B.; Redfern, P. C.; Teschner, D.; Pellin, M. J.; Curtiss, L. A.; Vajda, S. *Science* **2010**, *328*, 224−228.
(12) Liong, M.; France, B.; Bradley, K. A.; Zink, J. I. *Adv. Mater.* **2009**, *21*, 1684−1689.
(13) Rifai, S.; Breen, C. A.; Swager, T. M. *Chem. Mater.* **2006**, *18*, 21−25.
(14) Southward, R. E.; Thompson, D. W. *Adv. Mater.* **1999**, *11*, 1043−1047.
(15) Rubira, A. F.; Rancourt, J. D.; Caplan, M. L. *Chem. Mater.* **1994**, *6*, 2351−2358.
(16) Warner, J. D.; Pevzner, M.; Dean, C. J.; Kranbuehl, D. E.; Scott, S. T.; Thompson, D. W.; Southward, R. E. *J. Mater. Chem.* **2003**, *13*, 1847−1852.
(17) Matsuda, S. I.; Ando, S. *Polym. Adv. Technol.* **2003**, *14*, 458−470.
(18) Sawada, T.; Ando, S. *Chem. Mater.* **1998**, *10*, 3368−3378.
(19) Qi, S.; Wang, W.; Wu, D.; Wu, Z.; Jin, R. *Eur. Polym. J.* **2006**, *42*, 2023−2030.
(20) Qi, S.; Wu, Z.; Wu, D.; Wang, W.; Jin, R. *Chem. Mater.* **2007**, *19*, 393−401.
(21) Qi, S.; Wu, Z.; Wu, D.; Wang, W.; Jin, R. *Langmuir* **2007**, *23*, 4878−4885.
(22) Qi, S.; Wu, D.; Bai, Z.; Wu, Z.; Yang, W.; Jin, R. *Macromol. Rapid Commun.* **2006**, *27*, 372−376.
(23) Wu, Z.; Wu, D.; Yang, W.; Jin, R. *J. Mater. Chem.* **2006**, *16*, 310−316.
(24) Akamatsu, K.; Ikeda, S.; Nawafune, H. *Langmuir* **2003**, *19*, 10366−10371.
(25) Korchev, A. S.; Bozack, M. J.; Slaten, B. L.; Mills, G. *J. Am. Chem. Soc.* **2004**, *126*, 10−11.
(26) Yin, D.; Horiuchi, S. *Langmuir* **2005**, *21*, 9532−9539.
(27) Wang, T. C.; Chen, B.; Rubner, M. F.; Cohen, R. E. *Langmuir* **2001**, *17*, 6610−6615.
(28) Shibata, M.; Kuribayashi, M.; Uda, T. *J. Appl. Polym. Sci.* **2004**, *94*, 2164−2169.
(29) Yang, S.; Wu, D.; Qi, S.; Cui, G.; Jin, R.; Wu, Z. *J. Phys. Chem. B* **2009**, *113*, 9694−9701.
(30) Su, W.; Li, P. Y.; Yao, L. B.; Yang, f.; Liang, L. F *ChemPhysChem* **2011**, *12*, 1143−1147.
(31) Vicsek, T. *Fractal Growth Phenomena*; World Scientific: Singapore, 1992.
(32) Mathieu, M.; Pinary, H.; Louis, B. *Nano Lett.* **2003**, *3*, 1611−1615.
(33) Mathieu, M.; Suzanne, G.; Marie-Paule, P. *Adv. Mater.* **2002**, *14*, 1084−1085.
(34) Mathieu, M.; Suzanne, G.; Marie-Paule, P. *J. Phys. Chem. B* **2003**, *107*, 2466−2470.
(35) Tang, Z.; Zhang, Z.; Wang, Y.; Glotzer, C.; Nicholas, A. *Science* **2006**, *314*, 274−278.
(36) Ortelli, E. E.; Geiger, F.; Lippert, T.; Wokaun, A. *Appl. Spectrosc.* **2001**, *55*, 412−419.
(37) Song, R.; Xu, A.; Antonietti, M.; Cölfen, H. *Angew. Chem., Int. Ed.* **2009**, *48*, 395−399.
(38) Song, R.; Cölfen, H. *Adv. Mater.* **2010**, *22*, 1301−1330.